Protein *N*-glycans in healthy and sclerotic glomeruli in diabetic kidney disease

Dušan Veličković[1], John Shapiro[2], Samir V Parikh[2], Brad Rovin[2], Robert D. Toto[3], Miguel A. Vazquez[3], Emilio D. Poggio[4], John F. O'Toole[4], John R. Sedor[4], Theodore Alexandrov[5,6,7], Sanjay Jain[8], Markus Bitzer[9], Jeffrey Hodgin[9], Marija Veličković[1], Kumar Sharma[10], Christopher R. Anderton*[1,10], for the Kidney Precision Medicine Project

Affiliations: [1]Earth and Biological Sciences Directorate, Pacific Northwest National Laboratory, Richland, Washington; [2]Department of Nephrology, The Ohio State University, Wexner Medical Center, Columbus, Ohio; [3]Division of Nephrology, Department of Internal Medicine, University of Texas Southwestern Medical Center, Dallas, Texas; [4]Department of Nephrology and Hypertension, Cleveland Clinic, Cleveland, Ohio; [5]Structural and Computational Biology Unit, European Molecular Biology Laboratory (EMBL), Heidelberg, Germany; [6]Molecular Medicine Partnership Unit, European Molecular Biology Laboratory, Heidelberg, Germany; [7]BioStudio, BioInnovation Institute, Copenhagen, Denmark; [8]Department of Medicine, Washington University School of Medicine, St. Louis; [9]Department of Pathology, Michigan Medicine, University of Michigan, Ann Arbor, Michigan; [10]Division of Nephrology, Department of Medicine, University of Texas Health San Antonio, San Antonio, Texas

*Christopher.anderton@pnnl.gov

SIGNIFICANCE STATEMENT (111/120 words)

Changes in protein *N*-glycosylation pathways resulting from diabetic kidney disease (DKD) in the glomerulus remain unknown despite the involvement of these protein post-translational modifications in glomerular filtration. Multi-spatial and single-cell omics performed on biopsies from patients with DKD revealed five common *N*-glycan signatures of sclerotic glomeruli that significantly differ in abundance compared to healthy glomeruli. Observed enzymatic and transcriptomic changes reflect that the biosynthetic pathways that can make these specific post-translational modifications were also altered. Accordingly, these results suggest that a subset of *N*-glycans, and their relative abundance to one another, are characteristic of sclerotic glomeruli in DKD and enzymes involved in their biosynthesis may be used as potential therapeutic targets.

STRUCTURED ABSTRACT (249/250 words)

Background

Diabetes is expected to directly impact renal glycosylation, yet to date, there has not been a comprehensive evaluation of alterations in *N*-glycan composition in the glomeruli of patients with diabetic kidney disease (DKD).

Methods

We used untargeted mass spectrometry imaging to identify *N*-glycan structures in healthy and sclerotic glomeruli in FFPE sections from needle biopsies of five patients with DKD and three healthy kidney samples. Regional proteomics was performed on glomeruli from additional biopsies from the same patients to compare the abundances of enzymes involved in glycosylation. Secondary analysis of single nuclei transcriptomics (snRNAseq) data was used to inform on transcript levels of glycosylation machinery in different cell types and states.

Results

We detected 120 *N*-glycans, and among them identified twelve of these protein post-translated modifications that were significantly increased in glomeruli. All glomeruli-specific *N*-glycans contained an *N*-acetyllactosamine (LacNAc) epitope. Five *N*-glycan structures were highly discriminant between sclerotic and healthy glomeruli. Sclerotic glomeruli had an additional set of glycans lacking fucose linked to their core, and they did not show tetra-antennary structures that are common in healthy glomeruli. Orthogonal omics analyses revealed lower protein abundance and lower gene expression involved in synthesizing fucosylated and branched *N*-glycans in sclerotic podocytes. In snRNAseq and regional proteomics analyses, we observed that genes and/or proteins involved in sialylation and LacNAc synthesis were also downregulated in DKD glomeruli, but this alteration remained undetectable by our spatial *N*-glycomics assay.

Conclusions

Integrative spatial glycomics, proteomics, and transcriptomics revealed protein *N*-glycosylation characteristic of sclerotic glomeruli in DKD.

INTRODUCTION

Diabetic kidney disease (DKD) is the leading cause of disability-adjusted life years (DALYs) in chronic kidney disease (CKD), accounting for 30.7% of the total CKD DALYs[1]. A host of processes mediates the progression of diabetic nephropathy to end-stage kidney disease. Still, none is as important as the gradual, inexorable scarring of the renal glomerulus, known as glomerulosclerosis. Given this, many studies over the last few decades have attempted to elucidate the molecular mechanisms that lead to this chronic sclerosing condition so that effective therapies and preventative strategies can be developed. Glomerulosclerosis in diabetic nephropathy is caused by the accumulation of extracellular matrix (ECM) proteins in the mesangium, resulting in sclerosis manifested by diffuse or nodular changes[2]. The gaps in understanding the pathophysiology of worsening kidney function associated with diabetes calls for new perspectives in discovery research to provide novel diagnostic markers and therapy targets[3].

One promising target is glycan biosynthesis and protein glycosylation, as hyperglycemia is expected to directly impact the renal glycome. High circulating glucose levels alter the physiological equilibrium of many enzyme-driven (glycosylation) and direct chemical reactions (glycation). Consequently, changes at proteoglycans of the ECM occur and lead to charge-selective permeability of the glomerular basement membrane (GBM)[3]. However, there is limited knowledge on the direct impact of hyperglycemia on glycan biosynthetic processes in the kidney, such as *N*- and *O*-linked glycan post-translational modifications of glycoproteins during the onset of disease. The reason for this is that much of our knowledge of human glycans is confined to those glycans expressed in blood cells, plasma glycoproteins, and antibodies which may not reflect glycan changes within the kidney tissue itself[4, 5]. It has been shown that *O*-mannosyl glycans regulate glomerular filtration by mediating the interface between podocyte foot processes and the GBM[6]. Moreover, *N*-glycosylation is essential for the proper membrane localization of several essential component proteins (e.g., nephrin, podocin, and Crumbs2), enables their interactions with other molecules, and further sustains the glomerular filtration barrier function[7]. As such, revealing changes in these post-translational modifications at the cell specific and tissue functional unit level can directly link to disease progression and may even be used for therapeutic targets.

Historically, lectin array and liquid chromatography with optical detection were commonly used techniques for *N*-glycosylation analysis in kidney disease[8]. However, these approaches could not sufficiently characterize glycan structures, and they only provided limited *N*-glycan coverage and analytical throughput, which limited their use in biomarker discovery and mechanistic studies[9]. Currently, a key technique for *N*-glycosylation analysis is mass spectrometry (MS) due to its high sensitivity, high duty cycle, and ability to provide structural information on *N*-glycans, which are all needed to meet clinical requirements of *N*-glycosylation profiling in a large cohort studies[7]. More recently, the development of matrix-assisted laser desorption/ionization mass spectrometry imaging (MALDI-MSI) approaches for mapping the distributions of *N*-glycans across biological specimens has shown tremendous potential, in part because it can provide insights into the tissue heterogeneity of *N*-glycosylation[10]. This technique has led to discovery of aberrant *N*-glycan structures characteristic of specific disease states or anatomical regions and tissue functional units within tissues[11-14]. For example, in clear cell renal cell carcinoma, it has been shown that tumor regions have a low level of bisecting glycans and glycans with multiple fucoses compared to nontumor regions of the same tissue section[15]. Another study identified abnormal high mannose glycans distributed across all regions of the diseased kidney tissue in lupus nephritis patients [16].

Recently, our laboratory improved the MALDI-MSI sample preparation workflow, specifically the on-tissue digestion step that can lead to diffusion of the *N*-glycans from their native locations[17]. Our new method provided us the ability to reveal the fine spatial information on *N*-glycan distributions from human kidney biopsies, where we could confidently determine *N*-glycans characteristic of glomeruli, blood vessels, fibrotic regions, and tubules in a healthy human needle biopsy[17]. This method can provide us the ability to know the exact spatial origin and structure of a *N*-glycan, which can be crucial for using it as a specific target or prognostic marker in clinical treatments. Herein, we used this capability to identify glomerulosclerosis specific *N*-glycans as biomarkers, and in integration with single nuclei transcriptomics and regional proteomics to propose biosynthetic pathways that can be valuable targets for DKD treatments.

METHODS

Patients and sample collection

Kidney tissue blocks from five DKD patients were obtained from the Kidney Translational Research Center (KTRC) biorepository under a KPMP main protocol approved by the Washington University Institutional Review Board (IRB 201102312). Three healthy reference sample (Pilot sample 016, 020, and 024), and one QC sample (KPMP pilot sample 18-162) were also used in this study. Informed consent was obtained for the use of data and samples. The kidney tissue was dissected form the whole kidney (Percutaneous Needle Biopsy), and then formalin fixed, and paraffin embedded for *N*-glycan analyses following KPMP Biospecimen MOP. For regional proteomics and snRNA-seq analyses dissected kidney tissue was embedded fresh frozen in Optical Cutting Temperature (OCT) in cryomolds and stored at -80 °C till ready for experimental use[18]. Demographic, diabetes duration, eGFR and albuminuria characteristic for each patient whose tissue blocks were used in the study are provided in **Table S1** and the summary statistic in **Table 1.**

Mass spectrometry imaging of *N*-glycans

Step-by-step details can be found in protocols.io[19]. Briefly, FFPE blocks of human kidney biopsies in pair with a QC reference sample (KPMP pilot sample 18-162: tumor nephrectomy, healthy reference, female, 60-69 years) were sectioned at 7 µm thickness and mounted on indium tin oxide (ITO)-coated glass slides. Slides were heated at 60 °C, dewaxed by xylenes washing (2x 3 mins), and rehydrated in serial EtOH/water washings: 100 % EtOH (2x 1 min), 96 % EtOH (1 min), 70% EtOH (1 min), and water (2x 3 min). Slides were then subjected to antigen retrieval in boiling citraconic buffer (pH~3) for 30 min, as described previously[20]. PNGase F (N-Zyme Scientifics, 100 µg/mL) was sprayed over the slides using a M5 Sprayer (HTX Technologies, Chapel Hill, NC) at a 25 µl/min flow rate, 15 passes, a crisscross pattern, 1200 mm/min spray head velocity, and 3.0 mm track spacing. Slides were then placed in a preheated incubation chamber where a relative humidity of 89% was maintained by saturated water solution of KNO_3 and incubated for 2 h at 37 °C, as described previously[17].

After incubation, α-cyano-4-hydroxycinnamic acid (CHCA, Sigma-Aldrich), at a concentration of 7 mg/mL (50% ACN and 0.1% TFA in water (v/v)), was sprayed over the tissue sections using the M5 Sprayer with the following settings: 100 µL/min, 10 passes, a crisscross pattern, a velocity of 1300 mm/min, and 3.0 mm track spacing. MALDI-MSI experiments were performed using a 15 Tesla SolariX Fourier-transform ion cyclotron resonance mass spectrometer (FTICR-MS; Bruker Daltonics, Bremen, Germany) equipped with a dual ESI/MALDI ion source and a Smart-beam II Nd:YAG (355 nm) laser. The instrument was operated in

positive ion mode over an m/z range of 1,000–5,000 with an estimated resolving power of 120,000 at m/z 400. The target plate stepping distance (lateral resolution) was set to 35 µm. The ion m/z 1809.6393 ($[M+Na]^+$ of Hex5 dHex1 HexNAc4) was used as a lock mass for on-line calibration. Imaging data were acquired using FlexImaging (v 4.1, Bruker Daltonics).

Imaging data files were imported into the SCiLS software, exported to imzML, and the resulting .imzML and .ibd files were submitted to METASPACE for data processing, using the NGlycDB as the database[20]. METASPACE annotations and Periodic acid Schiff (PAS) stained post-MALDI microscopy images were imported back into SCILS software where discrimination analysis (receiver operating characteristic, ROC) between healthy and sclerotic glomeruli was performed to report areas under the curves (AUC) for each *N*-glycan signal. Herein, a sclerotic glomerulus was defined as a glomerulus with extensive obliteration of the tufts (**Figure S1**). To minimize instrument and experiment drifts, for *N*-glycan abundance comparison between different kidney biopsies, intensity of the specific *N*-glycan in the glomerulus was normalized with the intensity of the same *N*-glycan in the glomerulus of the reference sample that was analyzed in parallel.

Histochemical Staining

Post-MALDI-MSI staining was performed using the PAS method. Briefly, MALDI matrix was removed by submerging the slide for 2 min in 2 changes of 50% ACN in water (v/v). Sections were fixed for 10 min using 10% Neutral Buffered Formalin (NBF), following rinsing in 4 changes of tap water. Next, slides were placed in 0.5% periodic acid (in water) for 5 min, rinsed in 4 changes of tap water, and then incubated in Schiff's Reagent for 15 min, following rinsing in warm tap water for 5 min. Counterstaining was done by submerging the slides in Mayer's Hematoxylin for 3 min, following rinsing with Tris-Buffered Saline (TBS), and then with 4 changes of deionized water. Sections were dehydrated and then cleared by submerging in 4 changes of absolute alcohol and xylenes, respectively, for 2 min each change. The slide was cover-slipped using resinous mounting media and scanned using the uScopeMXII (Microscopes International) with 20× objective.

Regional proteomics tissue collection

Sections (10 µm) were cut from the OCT frozen tissue blocks and mounted on thermoplastic (polyethylenenapthalate covered) glass slides (Carl Zeiss MicroImaging). The blades and water bath were changed before each case. Slides were processed as previously described.[21] They were placed in a desiccator for at least one week. The slides were then rinsed with EtOH and MS grade water and subsequently dehydrated in EtOH (70%, 95%, and 100%), air dried and immediately used for laser capture on the PALM technology microdissection system. Sections were micro dissected under a 10× ocular lens. For each biopsy, glomerular and tubulointerstitial compartments were collected separately. The cut elements were catapulted into 25 µl of 0.5% Rapigest (Waters Corporation, MA, USA), resuspended in 50 mM ammonium bicarbonate, collected in a 0.2 ml tube, and stored at -80 °C until the time of protein retrieval. Samples were thawed briefly, boiled for 20 min, and then further heated at 60 °C for 2 hr. Trypsin was added in a ratio of 1:30 trypsin:protein assuming ~2 µg retrieved protein/10,000 isolated cells. After overnight incubation at 37 °C, formic acid was added to a final concentration of 30% and the suspension was incubated for 30 min at 37 °C to degrade and render the Rapigest compatible with LC-MS/MS analysis. The extracts were dried, and peptides were resuspended in 20 µL of a solution of 2% acetonitrile with 0.1% formic acid and sonicated for 1 min in a water bath sonicator at 4 °C to ensure peptide solubilization.

Peptide concentration was obtained at 280 nm absorbance using 1 µl of sample on a Nanodrop ND-1000 spectrometer.

Regional proteomics data acquisition and analysis

Liquid chromatography tandem-mass spectrometry (LC-MS/MS) analysis was performed with a Thermo Scientific Easy1200 nLC (Thermo Scientific, Waltham, MA) coupled to a tribrid Orbitrap Eclipse (Thermo Scientific, Waltham, MA) mass spectrometer. In-line de-salting was accomplished using a reversed-phase trap column (100 µm × 20 mm) packed with Magic C18AQ (5-µm 200Å resin; Michrom Bioresources, Auburn, CA) followed by peptide separations on a reversed-phase column (75 µm × 270 mm) packed with ReproSil-Pur C18AQ (3-µm 120Å resin; Dr. Maisch, Baden-Würtemburg, Germany) directly mounted on the electrospray ion source. A 180-min gradient using a two-mobile-phase system consisting of 0.1% formic acid in water (A) and 80% acetonitrile in 0.1% formic acid in water (B). The chromatographic separation was achieved over a 180 min gradient from 8 to 30% B over 180 min, 30 to 45% B for 10 min, 45 to 60% B for 3 min, 60 to 90% B for 2 min and held at 90%B for 10 min at a flow rate of 300 nL/minute. A spray voltage of 2300 V was applied to the electrospray tip in line with a FAIMS source using varied compensation voltage -40, -60, -80 V, while the Orbitrap Eclipse instrument was operated in the data-dependent mode, MS survey scans were in the Orbitrap (Normalized AGC target value 300%, resolution 120,000, and max injection time 50 ms) with a 3 sec cycle time and MS/MS spectra acquisition were detected in the linear ion trap (normalized AGC target value of 50% and injection time 20 ms) using HCD activation with a normalized collision energy of 27%. Selected ions were dynamically excluded for 60 sec after a repeat count of 1.

Glomerular and tubulointerstitial proteins were studied separately. Label-free quantitative mass spectrometry was performed using spectral counting. Prior to statistical comparisons the protein spectral counts were normalized across samples. Data analysis was performed using Proteome Discoverer 2.5 (Thermo Scientific, San Jose, CA). The data were searched against a Uniprot Human database (Uniprot UP000005640 March 7, 2021) that also included common contaminants (cRAPOME Jan 29, 2015). Searches were performed with settings for the proteolytic enzyme trypsin. Maximum missed cleavages were set to 2. The precursor ion tolerance was set to 10 ppm and the fragment ion tolerance was set to 0.6 Da. Dynamic peptide modifications included oxidation on methionine (+15.995 Da) and dynamic modifications on the protein N-terminus included acetyl (+42.011 Da), Met-loss (-131.040 Da on M) and Met-loss+Acetyl (-89.030 Da on M). Sequest HT was used for database searching. All search results were run through Percolator for scoring and identified peptides were filtered for 1% peptide-level false discovery rate using q value of 0.01. Normalized spectral counts were compared between the nephrectomy controls and diabetic cases. A ratio of the average spectral counts for the nephrectomy controls to diabetic cases was determined and used to report protein abundance in our case compared to controls.

Single nuclei transcriptomics RNA-seq annotations

We used the single nuclei sequencing (SnRNA-seq) data and cell type identities from the human kidney atlas data[22] generated by the Human BioMolecular Atlas Program (HuBMAP)[23] and the Kindey Precision Medicine Project (KPMP) consortia (https://cellxgene.cziscience.com/e/0b75c598-0893-4216-afe8-5414cab7739d.cxg/). Herein, we used the atlas tool to compare cellular expression of genes involved in *N*-glycan biosynthetic machinery.

RESULTS

Regional proteomics confirms the findings of healthy glomeruli-specific *N*-glycan markers

We first investigated if regional proteomics data can be used to explain our previous observation of *N*-glycan structures enriched in glomeruli of healthy human kidney tissue. In that study we reported lists of *N*-glycans that are highly co-localized with glomeruli and non-glomerular regions of healthy human kidney biopsies, revealing that *N*-glycans with sialylation and tetra-antennary motifs are significantly enriched, whereas bisecting GlcNAc structures are significantly depleted in healthy glomeruli, **Figure 1**[17]. Regional proteomic data of the histologically healthy glomeruli and heathy tubulointerstitium orthogonally validate the findings for branching and sialic glycans but do not provide evidence for bisecting glycans. Namely, the α-1,6-mannosylglycoprotein 6-β-N-acetylglucosaminyltransferase (MGAT5) enzyme, which catalyzes the biosynthesis of branched glycans, more specifically the β1,6-GlcNAc branch[24], is more abundant in glomeruli than tubules as indicated by glomeruli/tubulointerstitium ratio. Enzymes involved in sialylation of the terminal Gal[25], i.e., ST6GAL1 that mediates α2,6-linked sialylation, and ST3GAL6 that mediates α2,3-linked sialylation, are also more abundant in gloms compared to tubules. Our proteomic data reveal that glomeruli/tubulointerstitium ratio for ST3GAL6 is more than 2-fold higher than glomeruli/tubulointerstitium ratio for ST6GAL1, implying that sialylated glycans in glomeruli are mostly α2,3 anomers, which aligns with early lectin staining reports[26]. On the other hand, the enzyme involved in synthesis of bisecting N-glycans, MGAT3 (β-1,4-mannosyl-glycoprotein 4-β-N-acetylglucosaminyltransferase)[24], was not been detected in tubulointerstitial regions (nor the glomeruli) in our proteomics analyses. Despite this enzyme remaining undetected, we are confident about the presence of this *N*-glycan, as it has been already measured in high abundance from bulk kidney tissue[27], and our spatial approach enabled ascribing it as highly enriched in non-glomeruli parenchyma of healthy kidney biopsies.

Spatial *N*-glycomics revealed glycan structures specific for sclerotic glomeruli in DKD biopsies

We noted the presence of both histologically normal appearing as well as sclerotic glomeruli in our diseased kidney biopsies. We applied our spatially resolved *N*-glycomics approach to delineate the molecular state of these two types of glomeruli. To increase confidence in reporting systematic glycan patterns, changes characteristic of glomerulosclerosis and finding patient-specific changes, we analyzed five biopsies from five different DKD patients, and compared them with glomeruli from the three healthy kidney samples. This resulted in 108 glomeruli that were compared across our analyses, as each biopsy contained multiple glomeruli in different sclerotic states.

By using our optimized *N*-glycan MALDI-MSI workflow, which provides functional tissue unit resolution, minimizes signal delocalization[17], and increases confidence in *N*-glycan annotation[20], we identified 120 *N*-glycan compositions of protein post-translational modifications in DKD samples (**Table S2,** and in METASPACE: https://metaspace2020.eu/api_auth/review?prj=9b673a2c-4796-11ee-adaa-2b05b7cde6a6&token=0zJ3rZ8jvhEW). Of these, twelve *N*-glycan structures were highly enriched in glomeruli, and 5 *N*-glycans distinguished sclerotic from healthy glomeruli, **Figure 2**.

Three structural features were immediately observable in the composition of these *N*-glycans. First, all of these *N*-glycans contain a N-acetyllactosamine (LacNAc) epitope, which is an addition of Gal to the initiating GlcNAc via β1,4-Gal transferases (B4GALTs) and β1,3-GlcNAc transferases (B3GNTs)[28]. Second, sclerotic glomeruli are characterized with an additional set of glycans that ubiquitously lack fucose (Fuc).

Lastly, *N*-glycans upregulated in sclerotic glomeruli do not show tetra-antennary structures that are common in healthy glomeruli. Biochemically, these *N*-glycans are synthesized by the α-1,3-mannosyl-glycoprotein 4-β-*N*-acetylglucosaminyltransferase (MGAT4) and MGAT5 enzymes[24].

A detailed look into the spatial distribution of these glom-specific glycans is provided in **Figures 3 and S2**. **Figure 3A** shows entire biopsy section, where within a 300 µm x 300 µm microscopic region, we can visualize neighboring sclerotic and healthy glomeruli (**Figure 3G**) and detect their different *N*-glycome profiles—a benefit of employing our MALDI-MSI approach. Relative abundances of selected *N*-glycans that are discriminant for sclerotic and healthy glomeruli are displayed, where **Figure 3B-D** shows individual *N*-glycans distributions and **Figure 3E** their blended distribution. Herein, magenta pixels in **Figure 3E**, whose brightness correspond to the signal intensity of non-fucosylated, bi-antennary *N*-glycan are almost entirely absent from healthy glomeruli and spread over sclerotic glomeruli (and to a lesser extent in other sclerotic areas). Whereas green pixels, which the brightness corresponds to the intensity of branched, fucosylated *N*-glycan signals highly co-localize with healthy glomeruli. These same findings were observed in the other DKD biopsies analyzed (**Figure S3**). An ion image that shows normalized ratio of those two glycans is presented in **Figure 3F,** where we can visualize how this type of representation can be used to discriminant healthy from sclerotic glomeruli. The ratio of those unique non-fucosylated vs fucosylated glycans is relatively preserved across glomeruli in healthy biopsies and moreover, this ratio is not affected by aging, which does not mean that the overall glycosylation profile is not affected[29]. Specifically, our results from three healthy reference samples show that the age of the participant (in the span from 45-72 yrs.) does not affect the normalized ratio of these two specific glycans in the healthy glomeruli (**Figure 3H**). Whereas this ratio notably varies between individual glomeruli of DKD biopsies, which likely represents their different sclerotic state (**Figure 3H**). Statistical analysis comparing this normalized ratio between 27 sclerotic glomeruli from biopsies and 50 healthy glomeruli from healthy reference samples indeed shows that the ratio of (Hex:5 HexNAc:4 NeuAc:1) and (Hex:7 HexNAc:6 dHex:1) could be used as the biomarker of glomerulosclerosis (p is 1.99E-10, **Table S3**). In general, ratios higher than 1 could be taken as a potential marker of sclerotic glomeruli, whereas ratios above 2 indicate severe sclerosis of glomeruli, which could be visualized in inserts of **Figure 3H**. Using this metrics, we concluded that glomeruli of sample S-1905-017532 do not show sclerotic signatures, which was consistent with histology examination, **Figure S2**. Worth noting is that although the ratio between the specific non-fucosylated (Hex:5 HexNAc:4 NeuAc:1) and fucosylated (Hex:7 HexNAc:6 dHex:1) glycans is higher in sclerotic glomeruli, we can observe that many other fucosylated glycans are not discriminant between the two types of glomeruli (**Figure 2**).

Regional proteomic and single-nucleus transcriptomics data complement observed *N*-glycan changes in glomerulosclerosis

We sought to confirm if the observations from spatial glycomics can provide deeper insights into corresponding protein and gene expression regulation. Using the regional proteomic and snRNAseq data from the human kidney tissue atlas datasets[30], we can see a drop in FUT8 expression in glomeruli of DKD patients compared to healthy glomeruli (**Figure 4**). This correlates with our molecular imaging findings that there is a depletion of fucosylated *N*-glycans of the glycoproteins in sclerotic glomeruli (**Figure 3**). Moreover, MGAT5 expression is significantly decreased in DKD podocytes, resulting in a lower yield of tetra-antennary glycans in the glomeruli. As such, snRNA-seq data identified the potential cell source for the branching glycan modification in sclerotic glomeruli to a degenerative podocyte cell state. A MGAT5 protein abundance is also higher in glomeruli compared to tubules of DKD biopsies (i.e., protein

abundance ratio is higher than 1) that indicates branching *N*-glycans are still enriched in glomeruli of DKD biopsies, which we visualized in our *N*-glycan MALDI-MS imaging data as well (**Figure 3**). In general, it seems that entire machinery for complex *N*-glycan biosynthesis is presented in lower abundance in glomeruli from DKD biopsies compared to glomeruli from healthy biopsies. Based on the regional proteomics data, abundance of enzymes involved in LacNAc synthesis (B3GNT2 and B4GALT1) is significantly decreased in DKD glomeruli. However, neither snRNAseq nor spatial *N*-glycomics data demonstrate this trend, but rather this data shows an unchanged expression of genes and abundance of LacNAc *N*-glycans in glomeruli of healthy and DKD patients, respectively. Another discrepancy between the omics data was observed in terms of sialylation. Here, both proteomics and snRNAseq indicate significantly lower levels of these structures in DKD glomeruli, but our spatial *N*-glycomics assay did not capture these differences as a common pattern. In fact, the spatial *N*-glycomics data show that while this is true for specific sialylated *N*-glycans, such as those with tetra-antennary structures, some sialylated N-glycans are enriched in sclerotic glomeruli (**Figure 2**).

DISCUSSION

Implementing our MALDI-MSI workflow to identify unique *N*-glycans of sclerotic and healthy glomeruli in DKD biopsies shed new light on glycome aberrations of glycoproteins during glomeruloscleroses and provided potential molecular markers of pathogenesis. This was possible by the unique ability of the applied imaging technique via mass spectrometry, which permitted us to go beyond simple epitope discovery and provide insight into the exact molecular composition of specific structures and their relative abundance throughout sections obtained from a needle biopsy at ~25 µm spatial scale. Twelve *N*-glycans were found to be significantly enriched in glomeruli compared to other non-glomerular kidney parenchyma, all characterized by terminal galactose. This is a significant finding, as galactose residues serve important functions in *N*-glycosylated proteins, such as modulating immune response by masking or exposing epitopes to antibodies[31]. For example, changing the degree of galactosylation of IgG *N*-glycans was associated with glomerular filtration rate in individuals with type 2 diabetes, suggesting the involvement of the immune system in the pathology of diabetic nephropathy[32]. Second, *N*-glycans found to be increased in sclerotic glomeruli did not contain fucosylation. This discovery might be crucial, as core fucosylation is essential for the proper function of growth factor receptors[33]. Lastly, none of the *N*-glycans characteristic for sclerotic glomeruli have highly branched, tetra-antennary motifs. This is a key finding, as a previous study showed that treatment of mice with high concentrations of GlcNAc increases *N*-glycan branching and inhibits TCR activation in type 1 diabetes[34]. This is thought to result from a higher concentration of the cellular donor UDP (uridine 5'-diphosphate)–GlcNAc in the Golgi apparatus, which might increase the capacity of glycosyltransferases to produce GlcNAc linkages that contribute to *N*-glycan-branch formation[34].

Our MALDI-MS-based spatial N-glycomics approach does have a few notable limitations that prevented us from obtaining a deeper and more conclusive insight into glycosylation biochemistry of glomerulosclerosis. First, the spatial resolution is constrained to ~25 µm due to the laser spot size used, and the on-tissue enzymatic digestion does not permit us to resolve the exact cellular origin of the glycan aberrations inside glomerulus (i.e., podocytes, mesangial cells, endothelial cells). Second, detection of high mass sialic acid *N*-glycans might be compromised, due to a combination of their low abundance, negative charge, and/or the MALDI process causing in-source fragmentation. As such, we anticipate that other sialic acid *N*-glycans might also be discriminant between healthy and sclerotic glomeruli, especially because sialic acid glycans have been implicated in the formation of the glomerular filtration apparatus in

the kidney, where the dense array of negative charge keeps filtration slits open[35]. ~~Finally~~Third, this method cannot resolve *N*-glycans that have the exact same composition but different chemical structure (mass isomers) as only the exact mass (i.e., mass to charge (m/z)) of the molecules is measured by MS. Nevertheless, the canonical *N*-glycans backbone inherent in the N-glycan biosynthesis provide annotation of their tentative structures, but there are still compositions like bisecting *N*-glycans that could also be interpreted as triantennary glycans that involve a completely different set of enzymes in their biosynthesis. Linkage of sialic acid (i.e., α-2,6 or α-2,3) is another example, and although biological differences of sialic acid anomers are still not well understood, there is growing evidence of their heterogenous distribution and expression across the different cells and pathological states[36]. Similar is with identifying localization of fucoslytlation on the N-glycan, since fucose can be part of the core or the branch. MALDI-MS imaging alone cannot differentiate them, although some recent advancements in employing a different set of enzymes were quite successful in solving this isomeric ambiguity[37]. Finally, a relatively small sample size and lack of longitudinal studies in this study might have masked or inflated the value of specific glycan changes in CKD patients.

Integration of our MALDI-MS imaging molecular findings with regional proteomic and snRNAseq data permitted us to gain additional insights into glomerulosclerotic glycosylation, and to even overcome some of the MALDI-MS imaging limitations. Here, we should acknowledge that these three-omics are cross sectional analyses and that the gene expression and proteomic profiles presented may not represent the evolution of a glomerulosclerotic process captured in the spatial glycomics results. Still, several hypotheses can be made. In most cases there was high agreement between transcript, protein abundance, and end-product of enzyme activity (i.e., the *N*-glycans they synthesize). For example, there was high coherence in the data streams related to changes in core fucosylation and suppressed branching in DKD glomeruli. Herein, we could employ the advantages of snRNAseq to ascribe branched *N*-glycans modification in sclerotic glomeruli to degenerative podocyte cell state, and as such bypass challenges inherent in MALDI-MS spatial resolution. Even more, regional proteomic data revealed that the sialic glycans identified in healthy gloms in the MALDI-MSI data are more likely α-2,3 anomers, and that fucose is most likely linked to the core of *N*-glycans, resolving mass isomer ambiguities. Alternatively, for specific glycosylation pathways, there was not direct agreement between the three orthogonal omics modalities, at first glance. For example, the decreased sialylation and decreased galactose content in DKD glomeruli were suggested by snRNAseq and regional proteomics, but not molecular analysis. This might be consequence of detectability issues of MALDI-MSI, where we might not capture high mass, very low abundant *N*-glycans that are affected by these two genes/enzymes. Another explanation is that because both enzymes can flux to other biosynthetic pathways, namely *O*-glycans modifications and glycolipid biosynthesis[28, 38], it might be that other end-products of these glycosyltransferases, rather than protein N-glycosylation, are affected in DKD.

Overall, this illustrates why a comprehensive look to the end of the transcript-protein-metabolite loop is of utmost importance to identify the phenotypic state of glomeruli and target correct genes/enzymes for potential therapies. We also envision that applying transcriptomics datasets to some of the newly developed glycomics pathway analyses tools, such as Glycopacity[39], might enable more insights into the changed metabolic environment in diabetic kidney tissue and the impact this may be having on *N*-glycan expression. Silencing or knocking out the FUT 8 and other genes involved in the observed alterations could also provide information in the future on how those specific *N*-glycan affect glomeruli cell lines in DKD. Further development in the field, and most critically linking glycan signatures to the specific glycoprotein,

will eventually reveal the functional role of these *N*-glycan alterations. Nonetheless, herein we showed that our current method for measuring the ratio between specific non-fucosylated (m/z 1976.6587, Hex:5 HexNAc:4 NeuAc:1) and the specific fucosylated glycan (m/z 2539.9037, Hex:7 HexNAc:6 dHex:1) can be used for distinguishing sclerotic and healthy glomerulus and even degree of glomerulosclerosis.

DISCLOSURES

K.S. reports serving as consultant for Bayer, Sanofi, and receiving research support from Boerhinger-Ingelheim. R.D.T reports funding from NIDDK for the Kidney Precision Medicine Project. All other authors have nothing to disclose.

FUNDING

The Kidney Precision Medicine Project (KPMP) is supported by the National Institute of Diabetes and Digestive and Kidney Diseases through the following grants: UH3 DK114923, UH3 DK114920, UH3 DK114933, UH3 DK114937, UH3 DK114907, U2C DK114886.

ACKNOWLEDGMENTS

We thank the KPMP patient participants, Recruitment sites, Central Hub, and all the Tissue Recruitment Sites for many valuable discussions and feedback towards this effort. We are grateful to the KPMP Publications and Presentation committee for suggestions and review of this manuscript. A complete list of all KPMP members can be found at kpmp.org.

AUTHOR CONTRIBUTIONS

D.V. and C.R.A. conceptualized the study. Data curation was performed by D.V., S.J., and S.M.P. Formal analysis was performed by D.V., M.V., S.V.P., and B.R. Tissue was obtained through KPMP Tissue Recruitment Sites: R.D.T., M.A.V., E.D.P., J.F.T, J.R.S, and J.H. Funding was acquired from C.R.A., K.S., R.D.T., S.J. M.A.V., E.D.P., J.F.T, J.R.S, and J.H. Resources from K.S., T.A., R.D.T., S.J. M.A.V., E.D.P., J.F.T, J.R.S, and J.H. The first draft of the manuscript was written by D.V. with editing assistance from C.R.A. All authors contributed to editing and finalizing the manuscript.

DATA SHARING STATEMENT

The data that support the findings of this study are available in the methods of this article. MALDI-MS imaging data are provided at **https://metaspace2020.eu/api_auth/review?prj=9b673a2c-4796-11ee-adaa-2b05b7cde6a6&token=0zJ3rZ8jvhEW.** Further information and requests for resources and reagents are available from the corresponding author.

SUPPLEMENTAL MATERIAL

Fig S1. Microscopy images of sclerotic and healthy glomeruli from the biopsies analyzed in this manuscript.

Fig S2. Microscopy images of PAS stained FFPE sections of DKD biopsies analyzed in this manuscript.

Fig S3. High-resolution MALDI-MSI of discriminant N-glycans in DKD human biopsies from different donors.

Table S1. Demographics, diabetes duration, eGFR (glomerular filtration rate), and albuminuria for each patient whose kidney biopsy was used in this study.

Table S2. List of N glycans detected across DKD biopsies and annotated by METASPACE.

REFERENCES

1. Oliva-Damaso, N., Mora-Gutierrez, J. M.,Bomback, A. S.: Glomerular Diseases in Diabetic Patients: Implications for Diagnosis and Management. *J Clin Med* 2021**,** *10* (9).
2. Qian, Y., Feldman, E., Pennathur, S., Kretzler, M.,Brosius, F. C.: Mechanisms of glomerulosclerosis in diabetic nephropathy. *Diabetes* 2008**,** *57* (6), 1439-1445.
3. Ravida, A., Musante, L., Kreivi, M., Miinalainen, I., Byrne, B., Saraswat, M., et al.: Glycosylation patterns of kidney proteins differ in rat diabetic nephropathy. *Kidney Int* 2015**,** *87* (5), 963-974.
4. Testa, R., Vanhooren, V., Bonfigli, A. R., Boemi, M., Olivieri, F., Ceriello, A., et al.: N-Glycomic Changes in Serum Proteins in Type 2 Diabetes Mellitus Correlate with Complications and with Metabolic Syndrome Parameters. *Plos One* 2015**,** *10* (3).
5. Torok, R., Horompoly, K., Szigeti, M., Guttman, A., Vitai, M., Koranyi, L., et al.: N-Glycosylation Profiling of Human Blood in Type 2 Diabetes by Capillary Electrophoresis: A Preliminary Study. *Molecules* 2021**,** *26* (21).
6. Kopp, J. B.: Dystroglycan in the Molecular Diagnosis of the Podocytopathies. *Clin J Am Soc Nephro* 2009**,** *4* (11), 1696-1698.
7. Ren, W. F., Bian, Q.,Cai, Y.: Mass spectrometry-based N-glycosylation analysis in kidney disease. *Front Mol Biosci* 2022**,** *9*.
8. Bermingham, M. L., Colombo, M., McGurnaghan, S. J., Blackbourn, L. A. K., Vuckovic, F., Bakovic, M. P., et al.: N-Glycan Profile and Kidney Disease in Type 1 Diabetes. *Diabetes Care* 2018**,** *41* (1), 79-87.
9. Kawakita, C., Mise, K., Onishi, Y., Sugiyama, H., Yoshida, M., Yamada, M., et al.: Novel urinary glycan profiling by lectin array serves as the biomarkers for predicting renal prognosis in patients with IgA nephropathy. *Sci Rep-Uk* 2021**,** *11* (1).
10. Drake, R. R., Powers, T. W., Jones, E. E., Bruner, E., Mehta, A. S.,Angel, P. M.: MALDI Mass Spectrometry Imaging of N-Linked Glycans in Cancer Tissues. *Adv Cancer Res* 2017**,** *134*, 85-116.
11. Lee, Y. R., Briggs, M. T., Young, C., Condina, M. R., Kuliwaba, J. S., Anderson, P. H., et al.: Mass spectrometry imaging spatially identifies complex-type N-glycans as putative cartilage degradation markers in human knee osteoarthritis tissue. *Anal Bioanal Chem* 2022**,** *414* (26), 7597-7607.
12. Hawkinson, T. R., Clarke, H. A., Young, L. E. A., Conroy, L. R., Markussen, K. H., Kerch, K. M., et al.: In situ spatial glycomic imaging of mouse and human Alzheimer's disease brains. *Alzheimers Dement* 2022**,** *18* (10), 1721-1735.
13. Boyaval, F., Dalebout, H., Van Zeijl, R., Wang, W. J., Farina-Sarasqueta, A., Lageveen-Kammeijer, G. S. M., et al.: High-Mannose N-Glycans as Malignant Progression Markers in Early-Stage Colorectal Cancer. *Cancers* 2022**,** *14* (6).
14. Malaker, S. A., Quanico, J., Raffo-Romero, A., Kobeissy, F., Aboulouard, S., Tierny, D., et al.: On-tissue spatially resolved glycoproteomics guided by N-glycan imaging reveal global dysregulation of canine glioma glycoproteomic landscape. *Cell Chem Biol* 2022**,** *29* (1), 30-+.
15. Drake, R. R., McDowell, C., West, C., David, F., Powers, T. W., Nowling, T., et al.: Defining the human kidney N-glycome in normal and cancer tissues using MALDI imaging mass spectrometry. *J Mass Spectrom* 2020**,** *55* (4).
16. Alves, I., Santos-Pereira, B., Dalebout, H., Santos, S., Vicente, M. M., Campar, A., et al.: Protein mannosylation as a diagnostic and prognostic biomarker of lupus nephritis: An unusual glycan-neoepitope in systemic lupus erythematosus. *Glycobiology* 2021**,** *31* (12), 1709-1709.

17. Velickovic, D., Sharma, K., Alexandrov, T., Hodgin, J. B.,Anderton, C. R.: Controlled Humidity Levels for Fine Spatial Detail Information in Enzyme-Assisted N-Glycan MALDI MSI. *J Am Soc Mass Spectr* 2022**,** *33* (8), 1577-1580.
18. Lake, B. B., Chen, S., Hoshi, M., Plongthongkum, N., Salamon, D., Knoten, A., et al.: A single-nucleus RNA-sequencing pipeline to decipher the molecular anatomy and pathophysiology of human kidneys. *Nat Commun* 2019**,** *10*.
19. Velickovic, D., Sharma, K., Alexandrov, T.,Anderton, C. R.: Spatial N-glycomics with MALDI-MSI for human kidney tissue V.2. *protocols.io* 2022.
20. Velickovic, D., Becejac, T., Mamedov, S., Sharma, K., Ambalavanan, N., Alexandrov, T., et al.: Rapid Automated Annotation and Analysis of N-Glycan Mass Spectrometry Imaging Data Sets Using NGlycDB in METASPACE. *Anal Chem* 2021**,** *93* (40), 13421-13425.
21. Ayoub, I., Shapiro, J. P., Song, H. J., Zhang, X. L., Parikh, S., Almaani, S., et al.: Establishing a Case for Anti-complement Therapy in Membranous Nephropathy. *Kidney Int Rep* 2021**,** *6* (2), 484-492.
22. Lake, B. B., Menon, R., Winfree, S., Hu, Q. W., Ferreira, R. M., Kalhor, K., et al.: An atlas of healthy and injured cell states and niches in the human kidney. *Nature* 2023**,** *619* (7970), 585-+.
23. Jain, S., Pei, L., Spraggins, J. M., Angelo, M., Carson, J. P., Gehlenborg, N., et al.: Advances and prospects for the Human BioMolecular Atlas Program (HuBMAP). *Nat Cell Biol* 2023**,** *25* (8), 1089-1100.
24. Kizuka, Y.,Taniguchi, N.: Enzymes for N-Glycan Branching and Their Genetic and Nongenetic Regulation in Cancer. *Biomolecules* 2016**,** *6* (2).
25. Meng, L., Forouhar, F., Gao, Z., Ramiah, A., Moniz, H., Thieker, D., et al.: Enzymatic basis for N-glycan sialylation: structure of rat ST6GAL1 reveals conserved and unique features for glycan sialylation. *Glycobiology* 2013**,** *23* (11), 1373-1374.
26. Babal, P., Slugen, I., Danis, D., Zaviacic, M.,Gardner, W. A.: Sialic acid expression in normal and diseased human kidney. *Acta Histochem* 1996**,** *98* (1), 71-77.
27. Nakano, M., Mishra, S. K., Tokoro, Y., Sato, K., Nakajima, K., Yamaguchi, Y., et al.: Bisecting GlcNAc Is a General Suppressor of Terminal Modification of N-glycan. *Mol Cell Proteomics* 2019**,** *18* (10), 2044-2057.
28. Kadirvelraj, R., Yang, J. Y., Kim, H. W., Sanders, J. H., Moremen, K. W.,Wood, Z. A.: Comparison of human poly-N-acetyl-lactosamine synthase structure with GT-A fold glycosyltransferases supports a modular assembly of catalytic subsites. *J Biol Chem* 2021**,** *296*, 100110.
29. Cindric, A., Kristic, J., Kavur, M. M.,Pezer, M.: Glycosylation and Aging. *Adv Exp Med Biol* 2021**,** *1325*, 341-373.
30. Hansen, J., Sealfon, R., Menon, R., Eadon, M. T., Lake, B. B., Steck, B., et al.: A reference tissue atlas for the human kidney. *Sci Adv* 2022**,** *8* (23).
31. Piirainen, M. A., Salminen, H.,Frey, A. D.: Production of galactosylated complex-type N-glycans in glycoengineered Saccharomyces cerevisiae. *Appl Microbiol Biot* 2022**,** *106* (1), 301-315.
32. Singh, S. S., Heijmans, R., Meulen, C. K. E., Lieverse, A. G., Gornik, O., Sijbrands, E. J. G., et al.: Association of the IgG N-glycome with the course of kidney function in type 2 diabetes. *Bmj Open Diab Res Ca* 2020**,** *8* (1).
33. Fang, M., Kang, L., Wang, X. L., Guo, X. N., Wang, W. D., Qin, B. J., et al.: Inhibition of core fucosylation limits progression of diabetic kidney disease. *Biochem Bioph Res Co* 2019**,** *520* (3), 612-618.
34. Marth, J. D.,Grewal, P. K.: Mammalian glycosylation in immunity. *Nat Rev Immunol* 2008**,** *8* (11), 874-887.
35. Weinhold, B., Sellmeier, M., Schaper, W., Blume, L., Philippens, B., Kats, E., et al.: Deficits in Sialylation Impair Podocyte Maturation. *J Am Soc Nephrol* 2012**,** *23* (8), 1319-1328.
36. Doostkam, A., Malekmakan, L., Hosseinpour, A., Janfeshan, S., Roozbeh, J.,Masjedi, F.: Sialic acid: an attractive biomarker with promising biomedical applications. *Asian Biomed* 2022**,** *16* (4), 153-167.

37. West, C. A., Liang, H. Y., Drake, R. R.,Mehta, A. S.: New Enzymatic Approach to Distinguish Fucosylation Isomers of N-Linked Glycans in Tissues Using MALDI Imaging Mass Spectrometry. *J Proteome Res* 2020**,** *19* (8), 2989-2996.
38. Hao, Y., Crequer-Grandhomme, A., Javier, N., Singh, A., Chen, H., Manzanillo, P., et al.: Structures and mechanism of human glycosyltransferase beta 1,3-N-acetylglucosaminyltransferase 2 (B3GNT2), an important player in immune homeostasis. *Journal of Biological Chemistry* 2021**,** *296*.
39. Dworkin, L. A., Clausen, H.,Joshi, H. J.: Applying transcriptomics to study glycosylation at the cell type level. *Iscience* 2022**,** *25* (6).

Table 1. Summary of demographics, diabetes duration, eGFR (glomerular filtration rate) and albuminuria for patients whose kidney biopsies were used in this study. HR (healthy reference sample)

Characteristic	CKD	HR
Sex		
Female	3	0
Male	2	3
Age (Years)	64.5 ± 7.0	58.3 ± 13.5
Race		
Black or AA	~~2~~3	0
White, Other	~~3~~2	3
eGFR (mL/min/1.73m2)	44.5 ± 18.7	84 ± 41
Albuminuria (mg/g)	206 ± 444	0
Diabetes duration (Years)	20 ± 10	0

Figure Legend and Figures

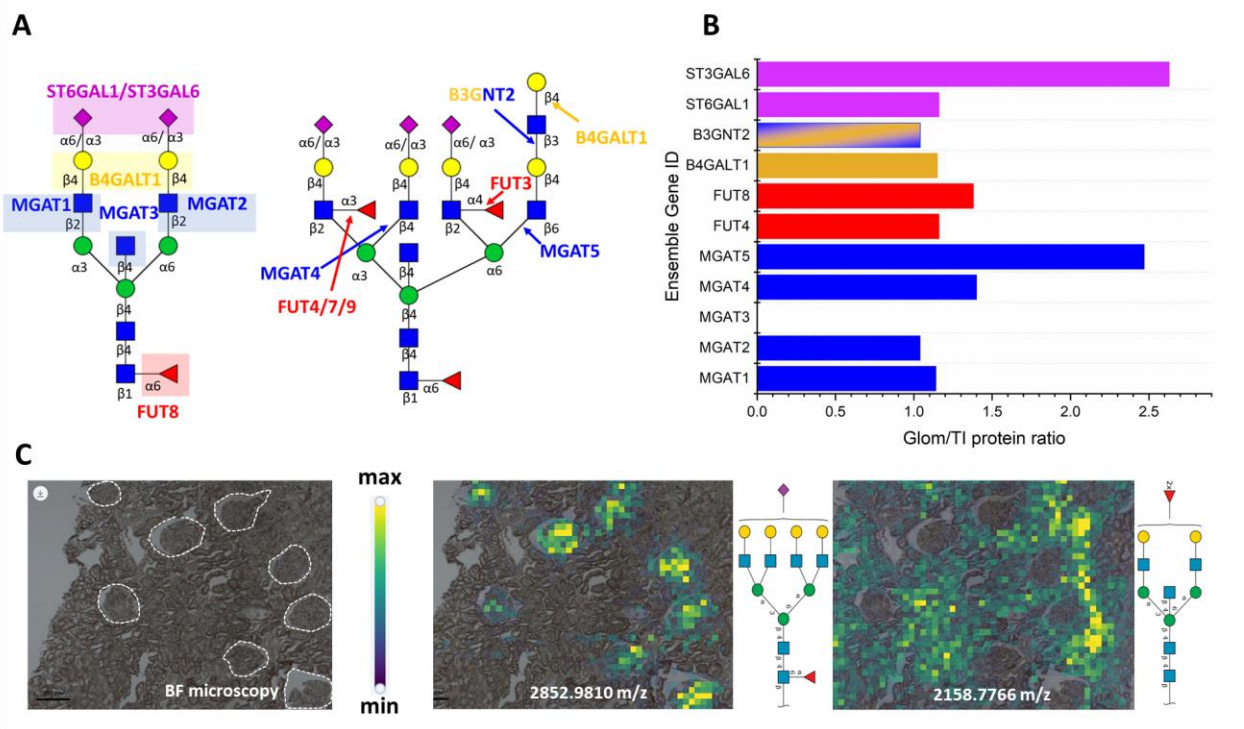

Figure 1. Spatial *N*-glycomics and regional proteomics of healthy reference kidney biopsies. (A) Genes involved in the specific biosynthetic steps during *N*-glycan maturation. (B) The regional proteomic table shows the relative ratio of enzymes involved in *N*-glycans' biosynthesis, between glomeruli and tubulointerstitial (TI) regions. (C) Brightfield microscopy (where white dashed lines outline glomeruli) and overlayed MALDI-MS ion images show the distribution of a sialylated tetra-antennary glycan (m/z 2852.9810) in gloms and a bisecting, non-sialylated *N*-glycan (m/z 2158.7766) in tubular regions outside of the gloms.

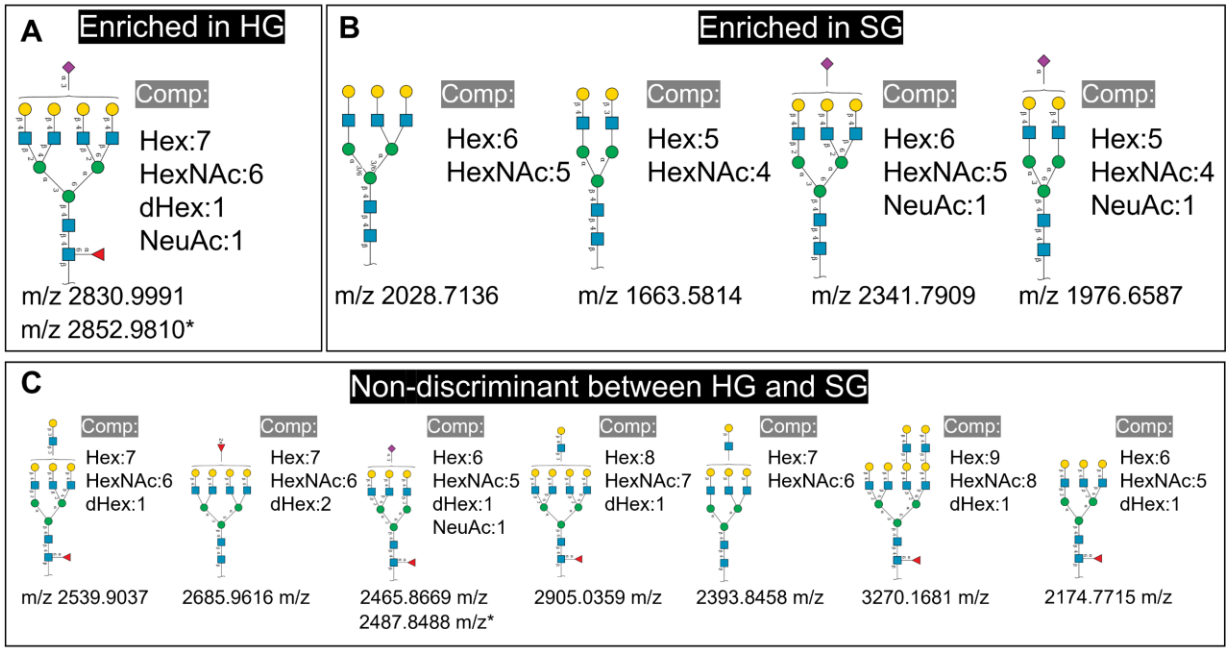

Figure 2. Composition (Comp), m/z values, and tentative structures of 12 glomeruli specific *N*-glycans that are (A) enriched is healthy glomeruli (HG) compared to sclerotic glomeruli (SG), (B) enriched in sclerotic compared to healthy glomeruli, and (C) equally abundant in healthy and sclerotic glomeruli. *Some sialic acid N-glycans are visualized at two m/z values that correspond to two different adducts ([M+Na], and [M-H+2Na]).

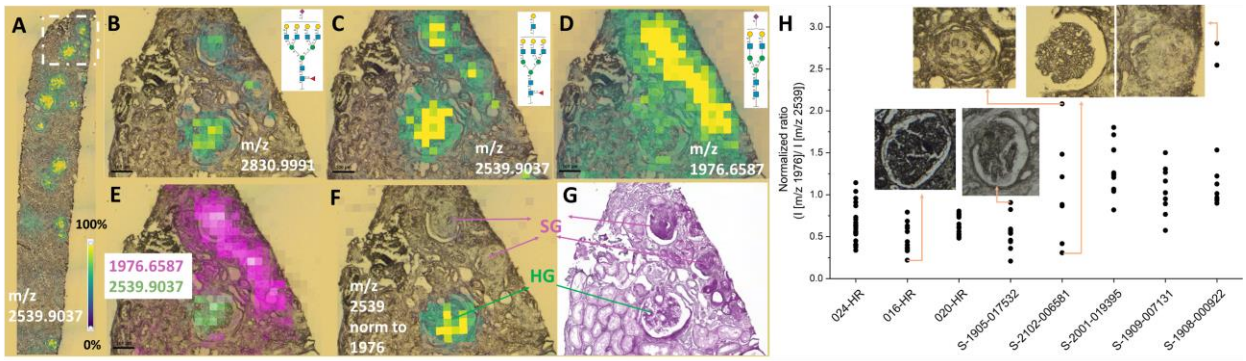

Figure 3. Example of high-resolution MALDI-MSI of *N*-glycans in DKD human biopsies. (A) Relative abundance of *N*-glycan at m/z 2539.9037 (Hex:7 HexNAc:6 dHex:1) over the entire kidney biopsy section (s-1908-000922). (B) Relative abundance of *N*-glycan (m/z 2830.9991; Hex:7 HexNAc:6 dHex:1 NeuAc:1) that is upregulated in healthy glomeruli (HG). (C) Relative abundance of *N*-glycan (m/z 2539.9037, Hex:7 HexNAc:6 dHex:1), which is non-discriminant between healthy and sclerotic glomeruli (SG). (D) Relative abundance of *N*-glycan (m/z 1976.6587, Hex:5 HexNAc:4 NeuAc:1) that is upregulated in sclerotic glomeruli. (E) Blended ion images of upregulated (magenta) and downregulated (green) *N*-glycans in sclerotic glomeruli. (F) Normalized ion image of m/z 2539.9037 N-glycan signal with m/z 1976.6587 N-glycan signal which clearly distinguishes healthy from sclerotic glomeruli. (G) Post MALDI PAS-stained microscopy image with clear visualization of neighboring sclerotic and healthy glomeruli. (H) The ratio of MS signal intensities at m/z 1976.6587 and m/z 2539.9037 in every glomerulus within the biopsies (there are multiple glomerulus per biopsy). The ratio of signals was normalized with corresponding ratio in reference sample that was run parallel with each biopsy. Microscopy images of gloms with the specific normalized ratio are presented as inserts. Pixel size of MALDI MSI images is 25µm by 25µm.

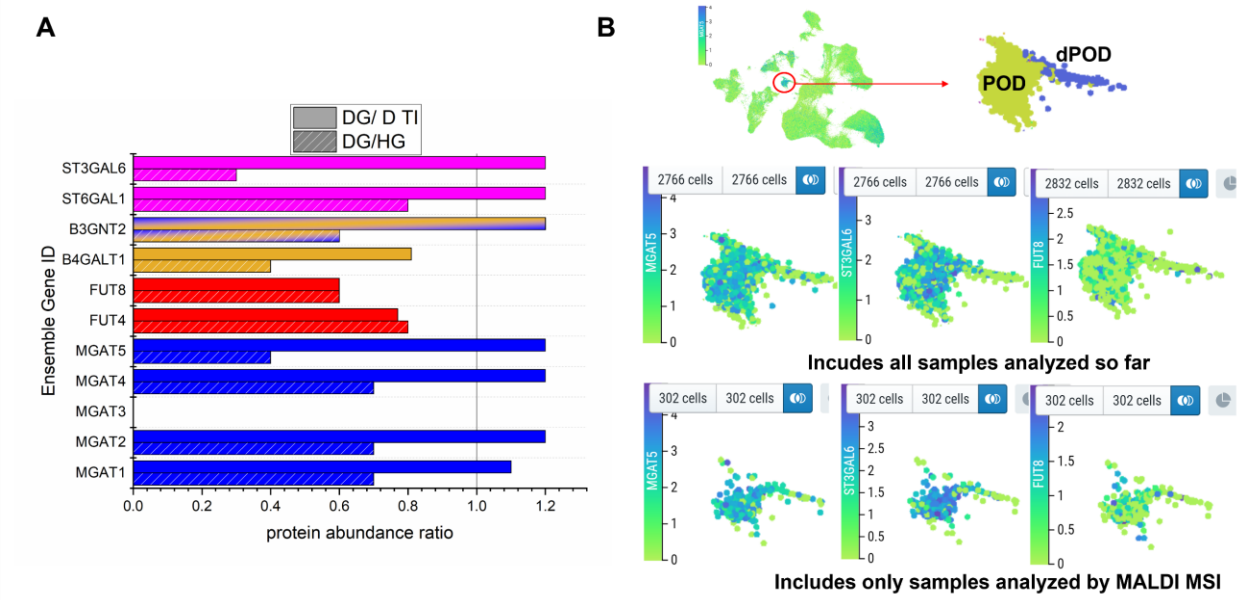

Figure 4. Comparative multiomics analysis of healthy and diseased kidney biopsies. (A) Regional proteomics data include averaged values of ratios between abundance in DKD (DG) and healthy glomeruli (HG), as well as DKD glomeruli and DKD tubulointerstitium (D TI). (B) An atlas of healthy and injured cell states and niches in the human kidney. SnRNAseq show the relative expression of selected genes in healthy (POD) and degenerative podocytes (dPOD) in all samples analyzed so far by snRNAseq as part of KPMP, and in a subgroup of patient samples whose biopsies were also analyzed by MALDI-MSI-based spatial *N*-glycomics.